Probing Strong-Field Physics in X-ray Emission from Magnetized Neutron Stars

Hoa Dinh Thi

In collaboration with:
Matthew G. Baring, Alice K. Harding, George A. Younes,
Rachael E. Stewart, Marcus E. Lower, Zorawar Wadiasingh

Theoretical Astroparticle and Cosmology Symposium in Texas (TACOS)
(October 23, 2026)

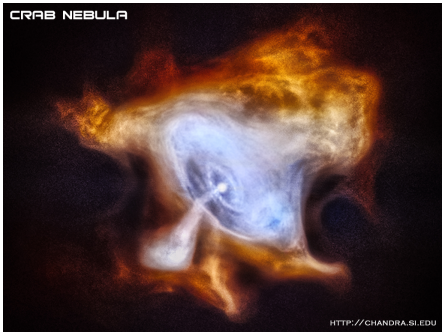


RICE UNIVERSITY

1. General Introduction

1.1 Neutron Stars: from Prediction to Discovery

Neutron stars: the "stellar zombies" left behind by massive stars.

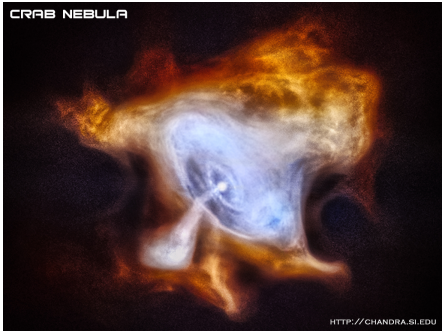


Crab Nebula

Credit: NASA/CXC/SAO

1.1 Neutron Stars: from Prediction to Discovery

Neutron stars: the "stellar zombies" left behind by massive stars.



Crab Nebula

Credit: NASA/CXC/SAO

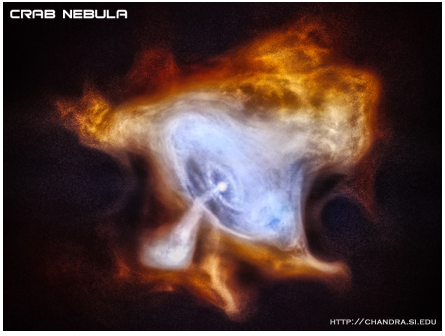
1934

Theoretical Prediction

Baade & Zwicky (Phys. Rev. 46, 76–77 (1934))

1.1 Neutron Stars: from Prediction to Discovery

Neutron stars: the "stellar zombies" left behind by massive stars.



Crab Nebula

Credit: NASA/CXC/SAO

1934

Theoretical Prediction

Baade & Zwicky (Phys. Rev. 46, 76–77 (1934))

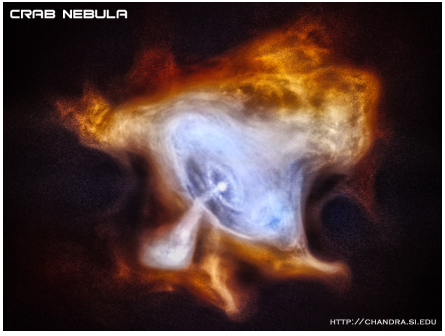
1967

First Pulsar Discovery

Bell & Hewish (Nature 217, 709–713 (1968))

1.1 Neutron Stars: from Prediction to Discovery

Neutron stars: the "stellar zombies" left behind by massive stars.



Crab Nebula

Credit: NASA/CXC/SAO

1934

Theoretical Prediction

Baade & Zwicky (Phys. Rev. 46, 76–77 (1934))

1967

First Pulsar Discovery

Bell & Hewish (Nature 217, 709–713 (1968))

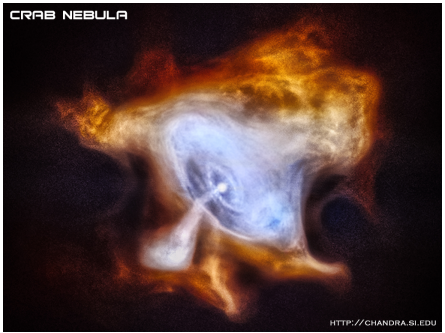
1968–1969

Pulsars Identified as Neutron Stars

Comella et al., Nature 221, 453–454 (1969)

1.1 Neutron Stars: from Prediction to Discovery

Neutron stars: the "stellar zombies" left behind by massive stars.



Crab Nebula

Credit: NASA/CXC/SAO

1934
Theoretical Prediction
Baade & Zwicky (Phys. Rev. 46, 76–77 (1934))

↓

1967
First Pulsar Discovery
Bell & Hewish (Nature 217, 709–713 (1968))

↓

1968–1969
Pulsars Identified as Neutron Stars
Comella et al., Nature 221, 453–454 (1969)

↓

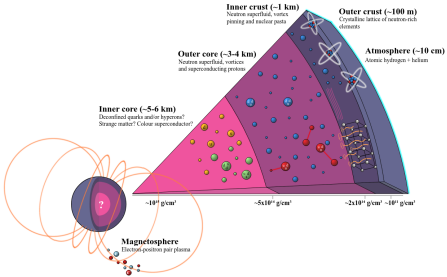
Nowadays
$\sim$ 4000 pulsars identified

1.2 Neutron Stars: the Most **Extreme** Stars Known in the Universe

Neutron stars are **extremely**

- **dense**:
  $M \sim 1-2\,M_\odot, R \sim 10-15\mathrm{km}, \rho_\mathrm{c} \gtrsim 5\rho_\mathrm{sat} \sim 10^{15}\mathrm{g/cm}^3$

Credit: Basu (2025)



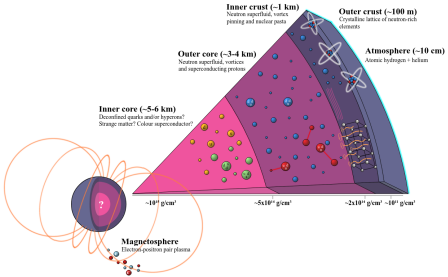
A NS and its magnetosphere

1.2 Neutron Stars: the Most **Extreme** Stars Known in the Universe

Neutron stars are **extremely**

- **dense**:
  $M \sim 1-2\,M_\odot, R \sim 10-15\mathrm{km}, \rho_c \gtrsim 5\rho_{\rm sat} \sim 10^{15}\mathrm{g/cm}^3$
  Different layers with different states of matter:
  crust (nuclei, n, e)$\rightarrow$ outer core (n,p, e, μ)$\rightarrow$inner core **(?)**

Credit: Basu (2025)



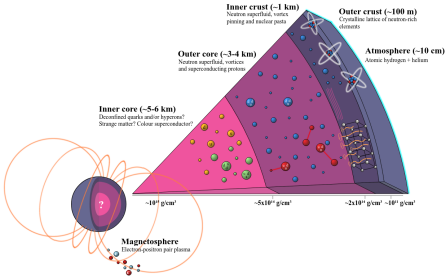
A NS and its magnetosphere

1.2 Neutron Stars: the Most **Extreme** Stars Known in the Universe

Neutron stars are **extremely**

- **dense**:
  $M \sim 1-2\,M_\odot, R \sim 10-15\mathrm{km}, \rho_c \gtrsim 5\rho_{\rm sat} \sim 10^{15}\mathrm{g/cm}^3$
  Different layers with different states of matter:
  crust (nuclei, n, e)$\rightarrow$ outer core (n,p, e, μ)$\rightarrow$inner core **(?)**
- **neutron-rich**: N $>$ 10 Z

Credit: Basu (2025)



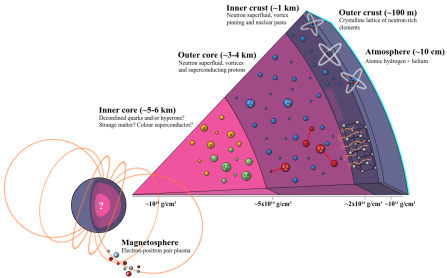
A NS and its magnetosphere

1.2 Neutron Stars: the Most **Extreme** Stars Known in the Universe

Neutron stars are **extremely**

- **dense**:
  $M \sim 1-2\,M_\odot, R \sim 10-15\mathrm{km}, \rho_c \gtrsim 5\rho_{\rm sat} \sim 10^{15}\mathrm{g/cm}^3$
  Different layers with different states of matter:
  crust (nuclei, n, e)$\rightarrow$ outer core (n,p, e, μ)$\rightarrow$inner core **(?)**
- **neutron-rich**: N $>$ 10 Z
- **hot** after birth:
  $T \sim 10^{11}$ K (newly born) $\rightarrow$ $T \sim 10^6$ K (old)

Credit: Basu (2025)



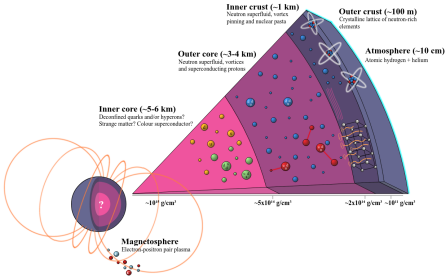
A NS and its magnetosphere

1.2 Neutron Stars: the Most **Extreme** Stars Known in the Universe

Neutron stars are **extremely**

- **dense**:
  $M \sim 1-2\,M_\odot, R \sim 10-15\mathrm{km}, \rho_c \gtrsim 5\rho_{\rm sat} \sim 10^{15}\mathrm{g/cm}^3$
  Different layers with different states of matter:
  crust (nuclei, n, e)→ outer core (n,p, e, μ)→inner core **(?)**
- **neutron-rich**: N $>$ 10 Z
- **hot** after birth:
  $T \sim 10^{11}$ K (newly born) $\rightarrow T \sim 10^6$ K (old)
- **magnetized**: $B \gtrsim 10^9$ Gauss
  📋 Diverse population, e.g., millisecond pulsars, pulsars, **magnetars** ($B \gtrsim 10^{14}$ Gauss)
  👉 induce extreme phenomena in the atmospheres and magnetospheres.

Credit: Basu (2025)



A NS and its magnetosphere

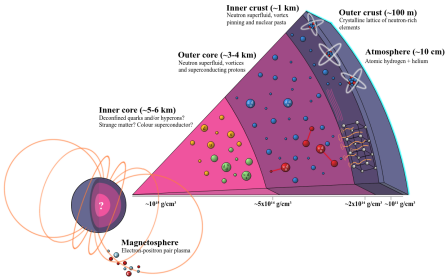
1.2 Neutron Stars: the Most **Extreme** Stars Known in the Universe

Neutron stars are **extremely**

- **dense**:
  $M \sim 1-2\,M_\odot, R \sim 10-15\mathrm{km}, \rho_c \gtrsim 5\rho_{\rm sat} \sim 10^{15}\mathrm{g/cm}^3$
  Different layers with different states of matter:
  crust (nuclei, n, e)→ outer core (n,p, e, μ)→inner core **(?)**
- **neutron-rich**: N $>$ 10 Z
- **hot** after birth:
  $T \sim 10^{11}$ K (newly born) $\rightarrow T \sim 10^6$ K (old)
- **magnetized**: $B \gtrsim 10^9$ Gauss
  📋 Diverse population, e.g., millisecond pulsars, pulsars, **magnetars** ($B \gtrsim 10^{14}$ Gauss)
  👉 induce extreme phenomena in the atmospheres and magnetospheres.

Opportunities for testing fundamental theories of physics

Credit: Basu (2025)



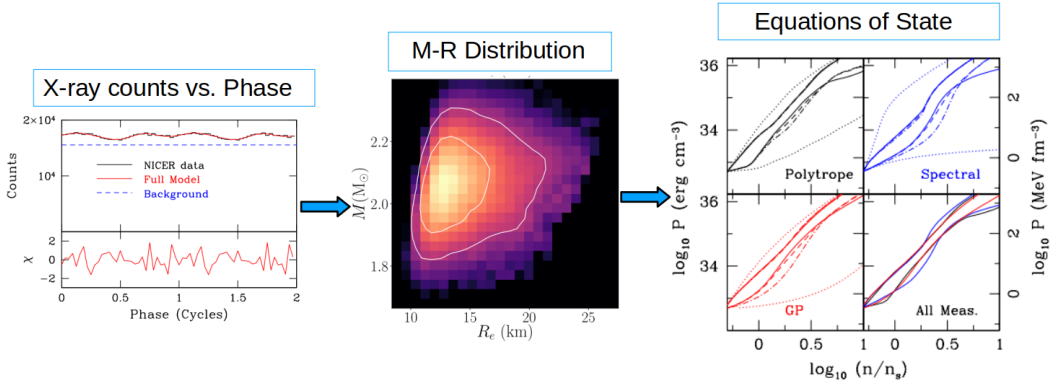
A NS and its magnetosphere

2. Motivations

2.1 Motivations (1)

Motivation 1

Soft X-ray Pulse Profiles → (M, R) → Equations of State → NS Interior Composition



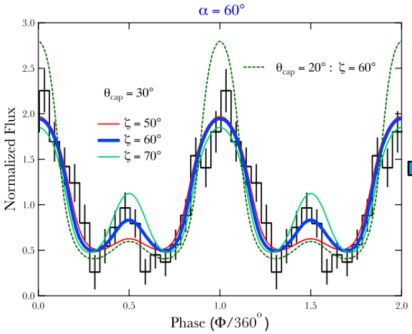
PSR J0740 + 6620 analysis by Miller et al. 2021 ApJL 918 L28

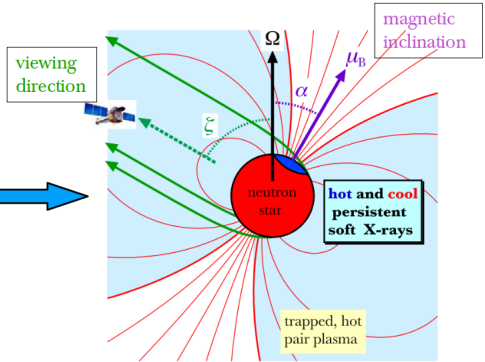
See also the analyses for PSR J0030+0451, PSR J0437-4715, PSR J0614–3329, PSR J1231−1411.

2.2 Motivations (2)

Motivation 2

Intensity PPs of X-rays provide constraints on NS geometry and hotspot properties.





Hu et al. 2023 IAU Symposium, 16(S363)

Hu et al. 2022 ApJ 928 82

(*See also* Gotthelf et al. 2010, Albano et al. 2010, Bernardini et al. 2011, etc.)

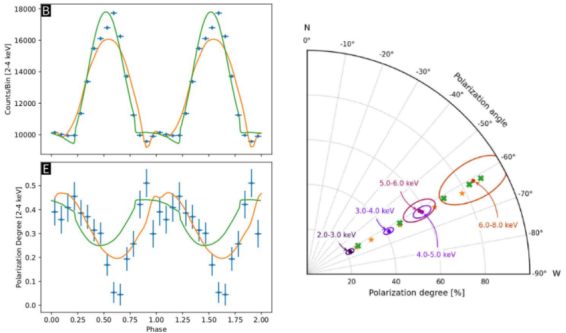
2.3 Motivations (3)

Motivation 3

IXPE polarization measurements provide further constraints on NS geometric parameters and allow probes of QED effects.

IXPE: Imaging X-ray Polarimetry Explorer

1RXS J1708−40 IXPE observation



- IXPE measures **Stokes Q, U**
  → Polarization degree:
  $\text{PD} = \sqrt{Q^2 + U^2}/I$
  → Polarization angle:
  $\text{PA} = \frac{1}{2} \arctan \frac{U}{Q}$
- Available for **7 magnetars**

Zane et al. 2023 ApJL 944 L27

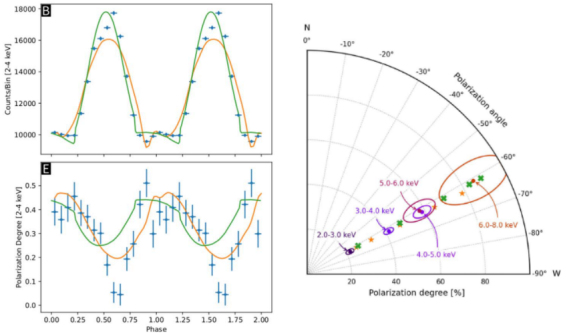
2.3 Motivations (3)

Motivation 3

IXPE polarization measurements provide further constraints on NS geometric parameters and allow probes of QED effects.

IXPE: Imaging X-ray Polarimetry Explorer

1RXS J1708−40 IXPE observation



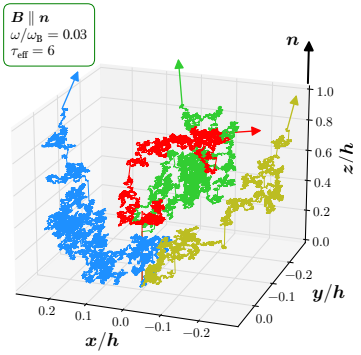
Zane et al. 2023 ApJL 944 L27

- IXPE measures **Stokes Q, U**
  → Polarization degree:
  $\mathrm{PD} = \sqrt{Q^2 + U^2}/I$
  → Polarization angle:
  $\mathrm{PA} = \frac{1}{2} \arctan \frac{U}{Q}$
- Available for **7 magnetars**

🎯 Our aim is to infer NS geometry, surface hotspots, as well as to probe QED effects by comparing simulated pulse profiles with data from observations.

3. Methods

3.1 Simulation of Radiative Transfer: MAGTHOMSCATT



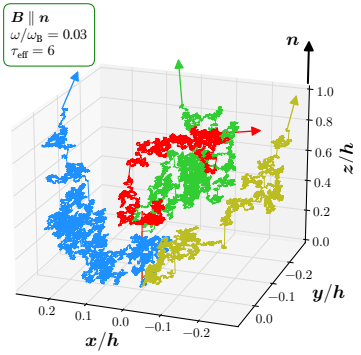
Dinh Thi, Baring, et al. 2025, ApJ 992 188

MAGTHOMSCATT

- **Monte Carlo code** for the polarized radiative transfer,

Barchas, Hu, Baring 2021 MNRAS 500, 5369
Hu, Baring, et al. 2022 ApJ 928 82

3.1 Simulation of Radiative Transfer: MAGTHOMSCATT



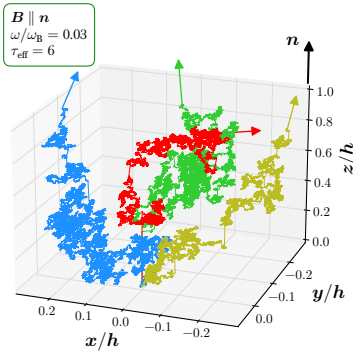
Dinh Thi, Baring, et al. 2025, ApJ 992 188

MAGTHOMSCATT

- **Monte Carlo code** for the polarized radiative transfer,
- **tracks complex electric field vectors** of photons →allows for capturing the complete polarization,

Barchas, Hu, Baring 2021 MNRAS 500, 5369
Hu, Baring, et al. 2022 ApJ 928 82

3.1 Simulation of Radiative Transfer: MAGTHOMSCATT



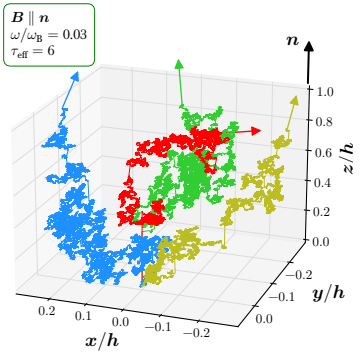
Dinh Thi, Baring, et al. 2025, ApJ 992 188

MAGTHOMSCATT

- **Monte Carlo code** for the polarized radiative transfer,
- **tracks complex electric field vectors** of photons →allows for capturing the complete polarization,
- has been **extensively validated** in different magnetic domains,

Barchas, Hu, Baring 2021 MNRAS 500, 5369
Hu, Baring, et al. 2022 ApJ 928 82

3.1 Simulation of Radiative Transfer: MAGTHOMSCATT



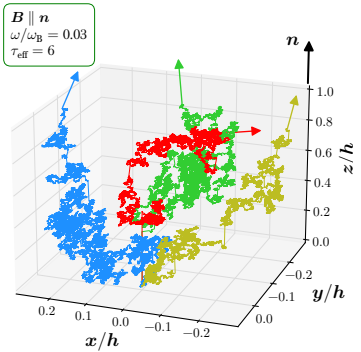
Dinh Thi, Baring, et al. 2025, ApJ 992 188

MAGTHOMSCATT

- **Monte Carlo code** for the polarized radiative transfer,
- **tracks complex electric field vectors** of photons →allows for capturing the complete polarization,
- has been **extensively validated** in different magnetic domains,
- incorporates **GR** and **QED** effects,

Barchas, Hu, Baring 2021 MNRAS 500, 5369
Hu, Baring, et al. 2022 ApJ 928 82

3.1 Simulation of Radiative Transfer: MAGTHOMSCATT



Dinh Thi, Baring, et al. 2025, ApJ 992 188

MAGTHOMSCATT

- **Monte Carlo code** for the polarized radiative transfer,
- **tracks complex electric field vectors** of photons →allows for capturing the complete polarization,
- has been **extensively validated** in different magnetic domains,
- incorporates **GR** and **QED** effects,
- **flexible**, can be applied to a wide variety of NSs.

Barchas, Hu, Baring 2021 MNRAS 500, 5369
Hu, Baring, et al. 2022 ApJ 928 82

3.2 Atmospheric Transport

Hu, Baring, Barchas, Younes 2022
ApJ 928 82

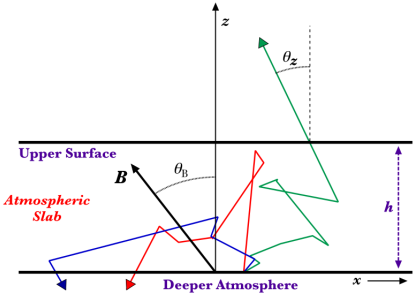


Illustration of a slab geometry

3.2 Atmospheric Transport

Hu, Baring, Barchas, Younes 2022
ApJ 928 82

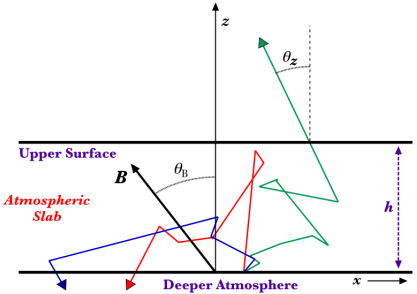
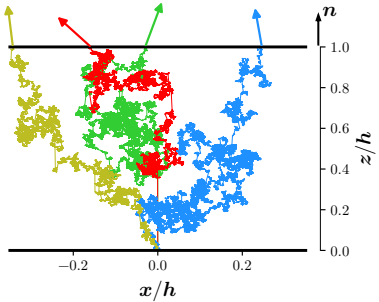


Illustration of a slab geometry

Dinh Thi, Baring, et al. 2025
ApJ 992 188



Trajectories in x-z plane from a real simulation

3.2 Atmospheric Transport

Hu, Baring, Barchas, Younes 2022
ApJ 928 82

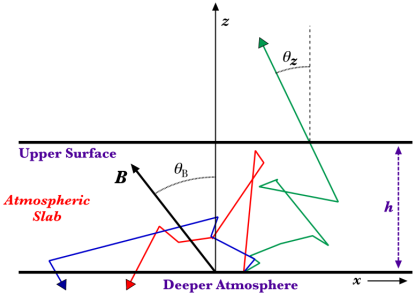
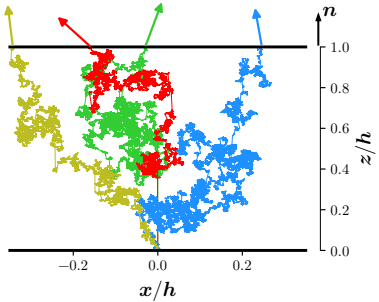


Illustration of a slab geometry

Dinh Thi, Baring, et al. 2025
ApJ 992 188

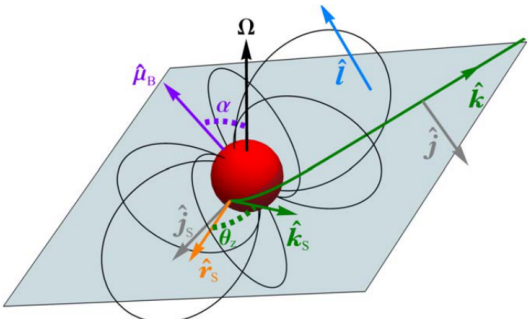


Trajectories in x-z plane from a real simulation

$$\vec{E} \Rightarrow \text{Stokes vector: } \mathbf{S} = (Q/I, U/I, V/I)$$

3.3 Magnetospheric Propagation to Observers (1)

General Relativity



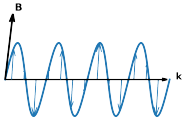
Propagation of light through the magnetosphere in the curved spacetime of the non-rotating Schwarzschild metric.

Hu, Baring, Barchas, Younes 2022 ApJ 928 82

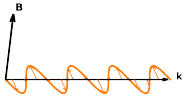
3.3 Magnetospheric Propagation to Observers (2)

Vacuum birefringence (VB) in the magnetosphere

O – mode:
E in the **k – B** plane



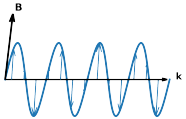
X – mode:
E perpendicular to the **(k – B)** plane



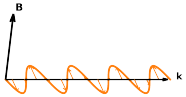
3.3 Magnetospheric Propagation to Observers (2)

Vacuum birefringence (VB) in the magnetosphere

O – mode:
E in the **k – B** plane



X – mode:
E perpendicular to the **(k – B)** plane



Evolution equation

$$i\begin{pmatrix}\frac{d\mathcal{E}_{\rm O}}{ds}\\ \frac{d\mathcal{E}_{\rm X}}{ds}\end{pmatrix} \approx \begin{pmatrix}\frac{-\omega\Delta n}{2c} & i\frac{d\Phi_{\rm B}}{ds}\\ -i\frac{d\Phi_{\rm B}}{ds} & \frac{\omega\Delta n}{2c}\end{pmatrix}\begin{pmatrix}\mathcal{E}_{\rm O}\\ \mathcal{E}_{\rm X}\end{pmatrix}$$

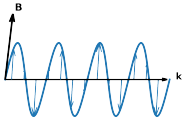
$$\Delta n = n_{\rm O} - n_{\rm X} = \frac{\alpha_{\rm f}}{4\pi}\frac{2}{15}\left(\frac{B}{B_{\rm cr}}\right)^2 \sin^2\theta_{\rm kB}$$

Adiabatic evolution: $\frac{\omega\Delta n}{2c} \gg |\frac{d\Phi_{\rm B}}{ds}|$.

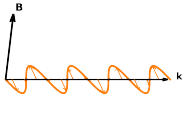
3.3 Magnetospheric Propagation to Observers (2)

Vacuum birefringence (VB) in the magnetosphere

O – mode:
E in the **k – B** plane



X – mode:
E perpendicular to the **(k – B)** plane



Evolution equation

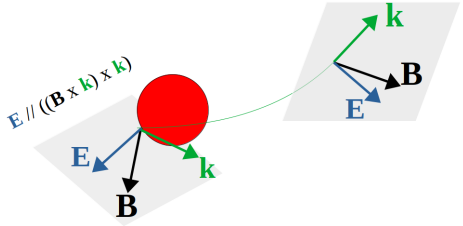
$$i\begin{pmatrix}\frac{d\mathcal{E}_{\rm O}}{ds}\\ \frac{d\mathcal{E}_{\rm X}}{ds}\end{pmatrix} \approx \begin{pmatrix}\frac{-\omega\Delta n}{2c} & i\frac{d\Phi_{\rm B}}{ds}\\ -i\frac{d\Phi_{\rm B}}{ds} & \frac{\omega\Delta n}{2c}\end{pmatrix}\begin{pmatrix}\mathcal{E}_{\rm O}\\ \mathcal{E}_{\rm X}\end{pmatrix}$$

$$\Delta n = n_{\rm O} - n_{\rm X} = \frac{\alpha_{\rm f}}{4\pi}\frac{2}{15}\left(\frac{B}{B_{\rm cr}}\right)^2 \sin^2\theta_{\rm kB}$$

Adiabatic evolution: $\frac{\omega\Delta n}{2c} \gg |\frac{d\Phi_{\rm B}}{ds}|$.

Adiabatic evolution of the polarization vector

Polarization vectors of photons propagating in a particular direction and polarization mode will align with each other

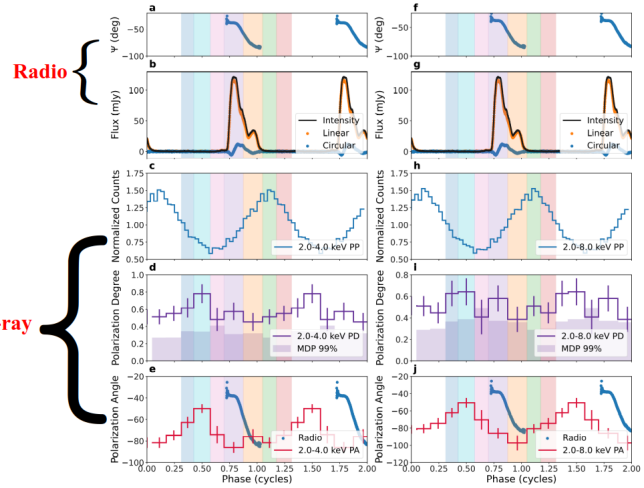


Evolution of the polarization vector in the **adiabatic** regime for a O-mode photon propagating through the magnetosphere.

4. Applications

4.1 Radio & X-ray Observations of Magnetar 1E 1547

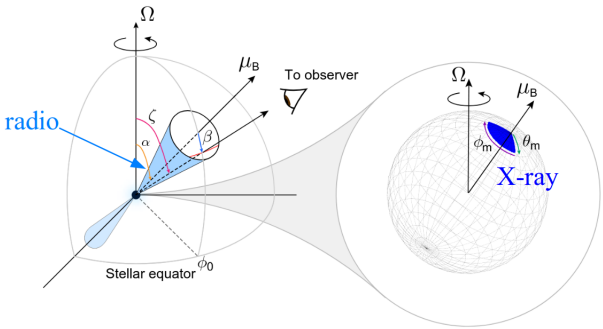
Stewart, Dinh Thi, Younes, Lower, Baring, et al.
Nature 2026, 656, 590-594



First joint intensity and polarization observations in both the **X-ray** (IXPE, NICER) and **radio** (Parkes/Murriyang) bands.

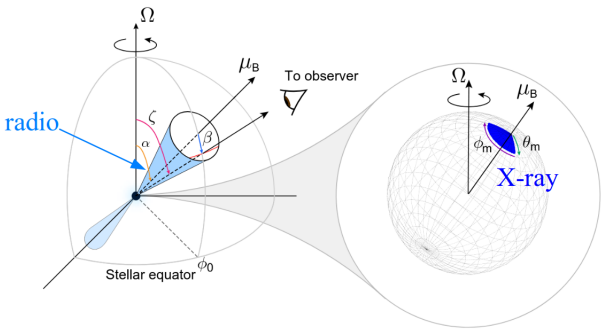
4.2 Radio Constraints on α, ζ

Stewart, Dinh Thi, Younes, Lower, Baring, et al. Nature 2026, 656, 590-594

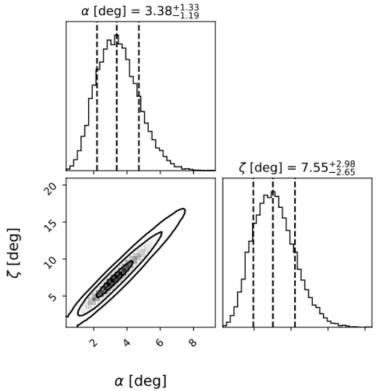


4.2 Radio Constraints on α, ζ

Stewart, Dinh Thi, Younes, Lower, Baring, et al. Nature 2026, 656, 590-594



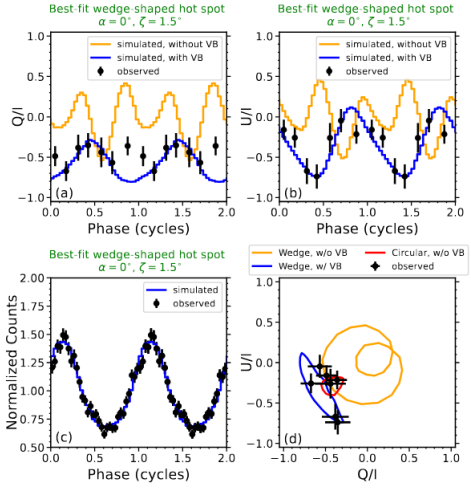
Radio Posterior



- $\alpha = 3.4^{\circ}{}^{+1.3}_{-1.2}$, $\zeta = 7.5^{\circ}{}^{+3.0}_{-2.6}$. 👉 **nearly-aligned rotator, viewed almost pole-on.**

4.3 X-ray Constraints

Stewart, Dinh Thi, Younes, Lower, Baring, et al.
Nature 2026, 656, 590-594

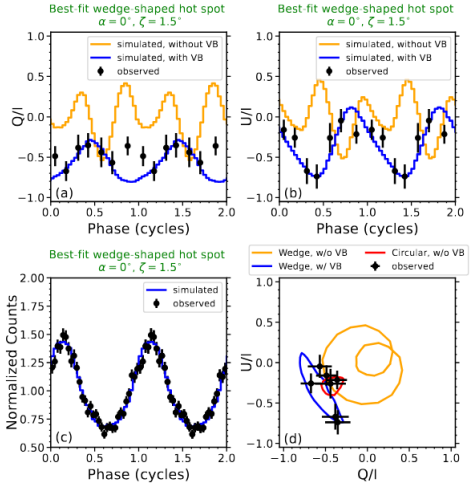


MAGTHOMSCATT Best-Fit Model:

- Wedge shaped hot spot
- **Aligned rotator** ($\alpha = 0^\circ$) and **viewed almost pole-on** ($\zeta = 1.5^\circ$)

4.3 X-ray Constraints

Stewart, Dinh Thi, Younes, Lower, Baring, et al.
Nature 2026, 656, 590-594



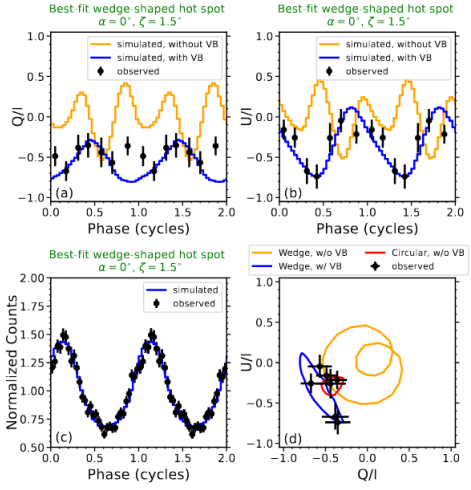
MAGTHOMSCATT Best-Fit Model:

- Wedge shaped hot spot
- **Aligned rotator** $(\alpha = 0°)$ and **viewed almost pole-on** $(\zeta = 1.5°)$

  👉 **Consistent with the radio-derived geometry**

4.3 X-ray Constraints

Stewart, Dinh Thi, Younes, Lower, Baring, et al.
Nature 2026, 656, 590-594



MAGTHOMSCATT Best-Fit Model:

- Wedge shaped hot spot
- **Aligned rotator** ($\alpha = 0°$) and **viewed almost pole-on** ($\zeta = 1.5°$)

  👉 **Consistent with the radio-derived geometry**
- Reproducing the X-ray polarization data requires **vacuum birefringence in the magnetosphere.**

4.4 Bayesian Analysis: Parameter Posteriors

"Semi-agnostic" Modeling

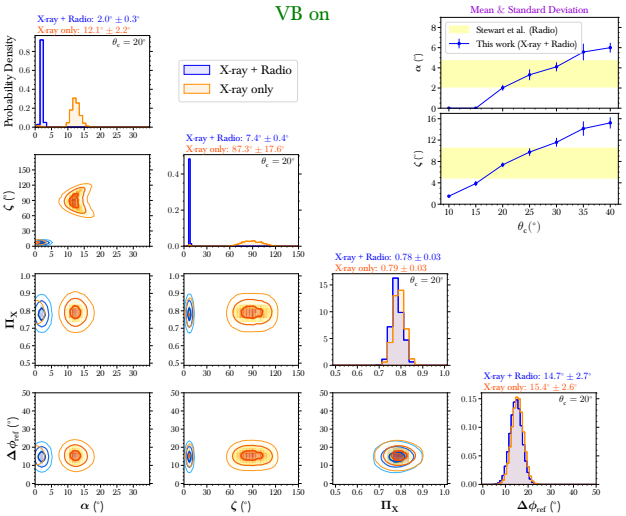
MAGTHOMSCATT polarization degree prediction is replaced by a free parameter, ranging from 0% to 100%.

X-ray only constraints:

- (α, ζ) exhibits bimodality: $\alpha \sim \mathbf{2}^\circ, \zeta \sim \mathbf{7}^\circ$ (consistent with radio-derived geometry) and $\alpha \sim \mathbf{10}^\circ, \zeta \sim \mathbf{90}^\circ$.

Joint X-ray and radio constraints:

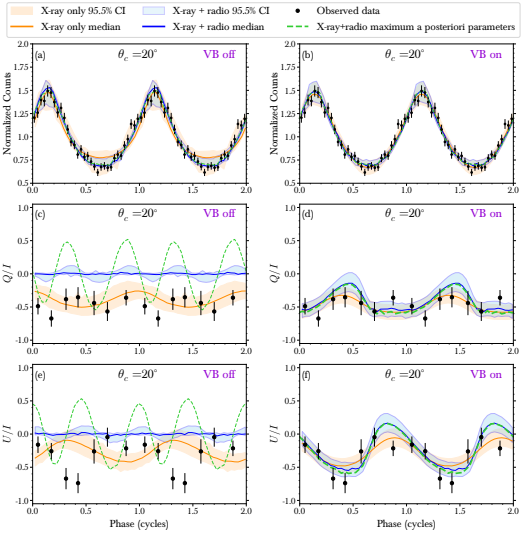
- $\alpha \sim \mathbf{2}^\circ, \zeta \sim \mathbf{7}^\circ$



Dinh Thi, Baring, et al., ApJ submitted

4.5 Bayesian Analysis: I,Q,U Posteriors

Dinh Thi, Baring, et al., ApJ submitted



Joint X-ray and radio constraints:

VB off (*left column*): Q and U exhibit only small oscillations around zero.

→**unable to reproduce the X-ray observations**.

👉 Reproducing the X-ray polarization data requires **VB on** (*right column*).

5. Conclusions

1. **Soft X-ray** pulse profiles from neutron stars encode information about their **geometric configuration** and **surface properties**.

5. Conclusions

1. **Soft X-ray** pulse profiles from neutron stars encode information about their **geometric configuration** and **surface properties**.
2. **Polarization measurements** from X-ray polarimetry missions, such as **IXPE**, can put **tighter constraints** these stellar geometric parameters.

5. Conclusions

1. **Soft X-ray** pulse profiles from neutron stars encode information about their **geometric configuration** and **surface properties**.
2. **Polarization measurements** from X-ray polarimetry missions, such as **IXPE**, can put **tighter constraints** these stellar geometric parameters.
3. IXPE observation also provide unique **probes of vacuum birefringence effects**.

5. Conclusions

1. **Soft X-ray** pulse profiles from neutron stars encode information about their **geometric configuration** and **surface properties**.
2. **Polarization measurements** from X-ray polarimetry missions, such as **IXPE**, can put **tighter constraints** these stellar geometric parameters.
3. IXPE observation also provide unique **probes of vacuum birefringence effects**.
4. The combined insights from recent X-ray and radio observations for **magnetar 1E 1547–5408** present indication for the presence the exotic QED prediction of vacuum birefringence.

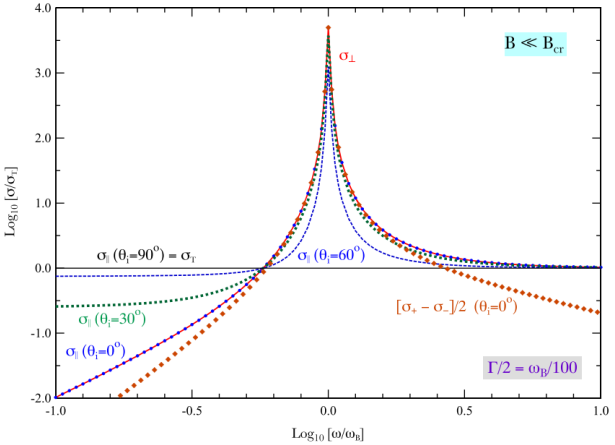
5. Conclusions

1. **Soft X-ray** pulse profiles from neutron stars encode information about their **geometric configuration** and **surface properties**.
2. **Polarization measurements** from X-ray polarimetry missions, such as **IXPE**, can put **tighter constraints** these stellar geometric parameters.
3. IXPE observation also provide unique **probes of vacuum birefringence effects**.
4. The combined insights from recent X-ray and radio observations for **magnetar 1E 1547–5408** present indication for the presence the exotic QED prediction of vacuum birefringence.
5. A careful treatment of the **mode conversion at the vacuum resonance** in the atmosphere is needed for magnetars and also for pulsars of weaker magnetizations.

Supplementary materials

Magnetic Thomson Cross Sections

Barchas, Hu, Baring 2021 MNRAS 500, 5369–5392



Polarization-dependent diff. CSs

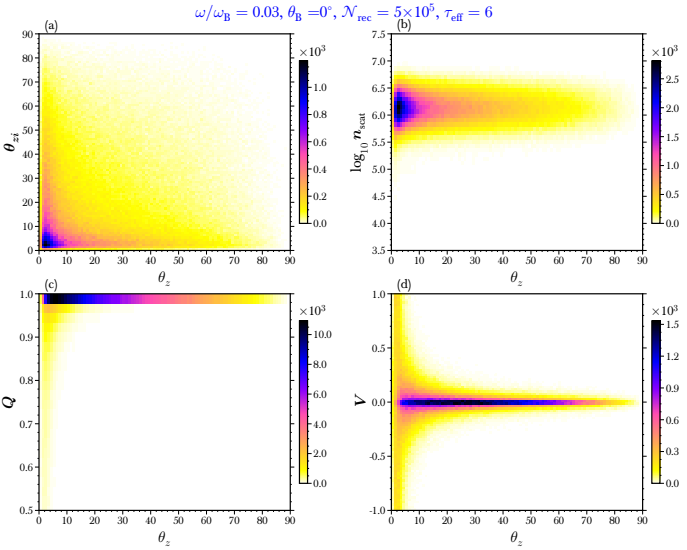
$$\frac{d\sigma_{\perp\to\perp}}{d\mu_f} = \frac{\pi r_0^2}{\left(\omega^2-\omega_{\rm B}^2\right)^2}\left(\omega^4+\omega^2\omega_{\rm B}^2\right)$$

$$\frac{d\sigma_{\perp\to\parallel}}{d\mu_f} = \frac{\pi r_0^2}{\left(\omega^2-\omega_{\rm B}^2\right)^2}\cos^2\theta_f\left(\omega^4+\omega^2\omega_{\rm B}^2\right)$$

$$\frac{d\sigma_{\parallel\to\perp}}{d\mu_f} = \frac{\pi r_0^2}{\left(\omega^2-\omega_{\rm B}^2\right)^2}\cos^2\theta_i\left(\omega^4+\omega^2\omega_{\rm B}^2\right)$$

$$\frac{d\sigma_{\parallel\to\parallel}}{d\mu_f} = 2\pi r_0^2\sin^2\theta_i\sin^2\theta_f + \frac{\pi r_0^2}{\left(\omega^2-\omega_{\rm B}^2\right)^2}\cos^2\theta_i\cos^2\theta_f\left(\omega^4+\omega^2\omega_{\rm B}^2\right)$$

Localized Annisotropy and Polarization in the Magnetar Domain



★ Magnetic scattering cone (MSC) angle:

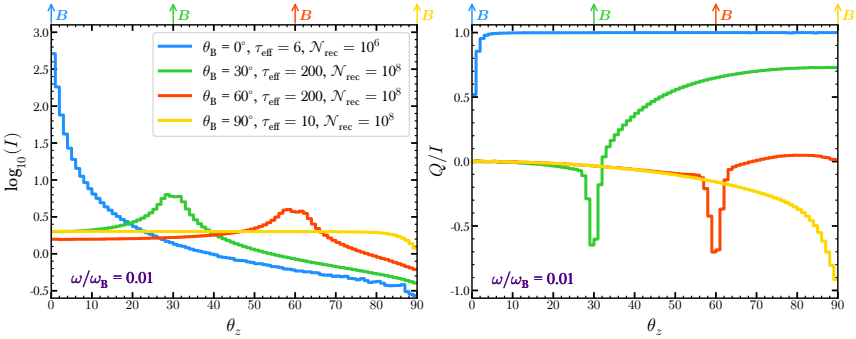
$$\theta_{\rm MSC} \equiv \omega/\omega_{\rm B} \ll 1.$$

- beaming along the field ($\theta_z \lesssim \theta_{\rm MSC}$).
- $\theta_z \gtrsim \theta_{\rm MSC}$: $Q \simeq 1$, $V \simeq 0$.

Baring et al. 2025 ApJ 982 126
Dinh Thi, Baring, et al. in prep.

Localized Annisotropy and Polarization in the Magnetar Domain

(Intensity and Stokes parameters are integrated over azimuthal angles around the zenith → $U = 0$.)



- The beaming around the magnetic field direction decreases when moving away from the pole.
- Although $|Q/I|$ is reduced to less than 100% in the mid-latitude and equatorial cases, the emission is dominated by $\|$-photons $\forall\theta_B$.